

Article

## Theoretical Analysis of the Catalytic Mechanism of *Helicobacter Pylori* Glutamate Racemase

Edgar Mixcoha, Mireia Garcia-Viloca, José M. Lluch, and Àngels González-Lafont

*J. Phys. Chem. B*, Just Accepted Manuscript • Publication Date (Web): 17 Sep 2012

Downloaded from <http://pubs.acs.org> on September 21, 2012

### Just Accepted

"Just Accepted" manuscripts have been peer-reviewed and accepted for publication. They are posted online prior to technical editing, formatting for publication and author proofing. The American Chemical Society provides "Just Accepted" as a free service to the research community to expedite the dissemination of scientific material as soon as possible after acceptance. "Just Accepted" manuscripts appear in full in PDF format accompanied by an HTML abstract. "Just Accepted" manuscripts have been fully peer reviewed, but should not be considered the official version of record. They are accessible to all readers and citable by the Digital Object Identifier (DOI®). "Just Accepted" is an optional service offered to authors. Therefore, the "Just Accepted" Web site may not include all articles that will be published in the journal. After a manuscript is technically edited and formatted, it will be removed from the "Just Accepted" Web site and published as an ASAP article. Note that technical editing may introduce minor changes to the manuscript text and/or graphics which could affect content, and all legal disclaimers and ethical guidelines that apply to the journal pertain. ACS cannot be held responsible for errors or consequences arising from the use of information contained in these "Just Accepted" manuscripts.



ACS Publications

High quality. High impact.

The Journal of Physical Chemistry B is published by the American Chemical Society. 1155 Sixteenth Street N.W., Washington, DC 20036  
Published by American Chemical Society. Copyright © American Chemical Society. However, no copyright claim is made to original U.S. Government works, or works produced by employees of any Commonwealth realm Crown government in the course of their duties.

1  
2  
3  
4  
5  
6  
7  
8  
9  
10  
11  
12  
13 Theoretical Analysis of the Catalytic Mechanism of  
14  
15     *Helicobacter pylori* Glutamate Racemase  
16  
17  
18  
19

20                     Edgar Mixcoha<sup>†</sup>, Mireia Garcia-Viloca<sup>†‡\*</sup>,  
21  
22                     José M. Lluch<sup>†‡</sup>, Àngels González-Lafont<sup>†‡\*</sup>  
23  
24  
25  
26

27     *Departament de Química and Institut de Biotecnologia i de Biomedicina,*  
28     *Universitat Autònoma de Barcelona, 08193, Bellaterra (Barcelona), Spain.*  
29  
30  
31  
32  
33  
34  
35  
36  
37  
38  
39  
40  
41  
42  
43  
44  
45  
46  
47  
48  
49  
50  
51  
52  
53

54                     \*Author to whom correspondence should be addressed. E-mail: mireia@klingon.uab.cat, an-  
55     gels@klingon.uab.cat  
56

57                     <sup>†</sup>Departament de Química.  
58

59                     <sup>‡</sup>Institut de Biotecnologia i de Biomedicina.  
60

## Abstract

One of the most challenging open key questions behind the stereoinversion of D-glutamate and L-glutamate catalyzed by glutamate racemases is how those enzymes manage to generate the thermodynamically unfavorable reverse protonation state of the catalytic residue cysteine required for the proton abstraction from the  $\alpha$ -carbon of glutamate. In this paper we have used Molecular Dynamics (MD) simulations with a Molecular Mechanics force field along with QM/MM calculations starting from the crystal structure and from different MD snapshots to study the enantiomeric conversion of D-glutamate to L-glutamate catalyzed by the *Helicobacter pylori* glutamate racemase. Our results show that structural fluctuations of the enzyme-substrate complex, represented by the different snapshots, lead to reactions paths with different features and fates. The whole reaction, when occurs, involves four successive proton transfers in three or four different steps. In the first step, Asp7 assists the deprotonation of D-glutamate by participating in general base catalysis with neutral Cys70 thiol. An analogous mechanism was previously found by some of us for the case of *Bacillus subtilis* glutamate racemase. This fact explains why that aspartate belongs to the group of strictly conserved residues.

## Keywords

*Helicobacter pylori* glutamate racemase, D-glutamate to L-glutamate interconversion , molecular dynamics simulation, enzyme catalysis, AM1-SRP/MM hybrid potencial.

## 1    Introduction

11 D-glutamate (DGL) is an essential component of the peptidoglycan layer of bacte-  
12 rial cell walls. Bacteria directly generate DGL from L-glutamate (GLU) via a class  
13 of enzymes called glutamate racemases (MurI/RacE) that have become a target for  
14 antibacterial drug discovery [1, 2, 3]. Glutamate racemases (EC 5.1.1.3) catalyze the  
15 reversible stereoinversion of GLU and DGL via a molecular mechanism that involves  
16 deprotonation of the glutamate  $\alpha$ -proton, followed by substrate reprotonation on the  
17 opposite stereochemical face. These proteins employ a two-base strategy with a cys-  
18 teine dyad serving as the acid-base pair [4, 5]. The abstraction of the  $\text{C}\alpha$ -hydrogen of  
19 amino acids poses a great challenge due to their low acidity and several different pro-  
20 posals on how the enzyme environment might be preorganized in an optimal manner  
21 for transition-state stabilization have been proposed [6, 7].

31      In previous papers [8, 9, 10], we have studied *Aquifex pyrophilus* glutamate race-  
32 mase (ApMurI). Our Molecular Dynamics (MD) calculations [8] supported the zwit-  
33 terionic DGL activation mechanism proposed by Richard and co-workers [11, 12]. In  
34 ApMurI [13, 14] the main chain  $\alpha$ -carboxylate of the substrate in a given monomer  
35 interacts with the residue Glu147' (that belongs to the other monomer) and Glu147'  
36 activates the substrate by a proton transfer. We also analyzed [10] the viability of  
37 the mechanism, firstly proposed by Glavas and Tanner [6], in which the Asp7 residue  
38 (ionized) could assist the deprotonation of DGL by participating in general base  
39 catalysis with neutral Cys70 thiol. In fact, the experimental mutation of that aspar-  
40 ate residue had resulted in a 1000-fold reduction of the observed  $k_{cat}$  of glutamate  
41 racemase [6]. Our MD simulations with this model revealed that Asp7 is the only  
42 residue close enough to interact with Cys70.

53      In a later work [15], we selected *Bacillus subtilis* glutamate racemase (BsRacE)  
54 to further analyze the molecular details of the DGL  $\rightarrow$  GLU catalytic reaction. The  
55 quaternary structure and the active sites of BsRacE and ApMurI are rather differ-  
56 ent.

1  
2  
3  
4  
5  
6  
7  
8  
9  
10  
11  
12  
13  
14  
15  
16  
17  
18  
19  
20  
21  
22  
23  
24  
25  
26  
27  
28  
29  
30  
31  
32  
33  
34  
35  
36  
37  
38  
39  
40  
41  
42  
43  
44  
45  
46  
47  
48  
49  
50  
51  
52  
53  
54  
55  
56  
57  
58  
59  
60

ent so another strategy to stabilize the carbanionic intermediate of the racemization reaction must be taking place in BsRacE. In fact, BsRacE crystal structure presents the conserved thiol dyad, Cys74 and Cys185, close to the side chains of Asp10 and His187 so then a four-hydrogen transfer mechanism involving two neutral cysteines assisted by one deprotonated aspartate and one doubly protonated histidine residue, could be possible. We carried out MD simulations of the BsRacE/DGL Michaelis complex and an exploration of the QM/MM potential energy surface at the AM1-SRP/MM level [16] to analyze the structural and energetic characteristics of the racemization process. Our results confirmed that the whole catalytic reaction involves four consecutive proton transfers that occur in three different steps. In the Michaelis complex the two cysteines are neutral but the ensemble of generated configurations of the BsRacE/DGL complex reveals that the system is prepared for the first proton transfer (deprotonation of Cys74 by Asp10). Once Cys74 is deprotonated the enantiomeric inversion of the  $\alpha$ -carbon involving two proton transfers (from the  $\alpha$ -carbon to Cys74 and from Cys185 to the  $\alpha$ -carbon) takes place in a concerted manner although highly asynchronous. Finally, in the third step, the nascent deprotonated Cys185 is protonated by His187. In addition, we also observed the key role of the positively charged  $-\text{NH}_3^+$  group of the substrate that stabilizes the system along the complete AM1/SRP reaction path by efficiently accompanying each proton transfer in a concerted and coupled way, but moving itself in the opposite direction.

In a concomitant paper, Spies *et al.* [17] carried out site-directed mutagenesis experiments and kinetic analysis as well as computational studies also on BsRacE. According to the authors, the reactive form of BsRacE/DGL, ready for the H-abstraction from  $\text{C}\alpha$ , cannot be the conformation of the BsRacE/DGL complex in the crystal structure. For that reason they argued that an MD simulation initiated from that crystal structure could never generate reactive configurations for the  $\text{D} \rightarrow \text{L}$  enantiomeric inversion. So then, their strategy to generate those reactive configurations

1  
2  
3  
4  
5  
6  
7  
8 consisted in developing an MM parametrized force field to carry out direct molecular  
9 dynamics of the glutamate carbanionic intermediate. These results were used by the  
10 authors for exploiting the transition-state binding energy of glutamate racemase in  
11 ligand discovery, and several effective competitive inhibitors were proposed based on  
12 a “cyclic” form of DGL [18]. However, no quantitative data corresponding to the  
13 energetic cost of reaching those “reactive” configurations of the enantiomeric process  
14 is given. Moreover, neither the viability of an assisted mechanism nor a justification  
15 for the thiolate form of Cys74, which is not the dominant protonation state at the  
16 catalytic pH, is discussed. On the other hand, in a very recent study on *Bacillus*  
17 *anthracis*, Whalen *et al.* [19] obtained the distribution of pK<sub>a</sub> values for Cys74 in  
18 the BsRacE/DGL system. In that study the authors highlight that the large fluctua-  
19 tions of the calculated pK<sub>a</sub>s of the catalytic base are due to a variety of interactions  
20 between the active site residues, particularly the interaction of Cys74 with Asp11. It  
21 is concluded that the primary driver of the catalytic power of glutamate racemase  
22 might be the so-called “reverse protonation state” (very high pK<sub>a</sub> thiol) as it has  
23 already been proposed for enolases [20] and alanine racemases [21, 22].  
24  
25

26 The enantiomeric inversion step of other racemases have also been reported. In the  
27 case of proline racemase, [23] the authors carried out the first free energy calculation  
28 in a PLP independent racemase using classical umbrella sampling techniques with  
29 stochastic boundary conditions based on an AM1-SRP/MM hybrid potential. The  
30 enantiomeric inversion was confirmed to be a concerted highly asynchronous two-proton  
31 transfer process in which the carbanionic intermediate was denominated a transient  
32 species. It is highlighted that only the two cysteines residues take part in the catalytic  
33 mechanism whereas Asp296 and His132 play structural roles and are crucial for the  
34 racemization charge migration. As the same authors indicate, the open question is the  
35 base responsible for the initial deprotonation of the cysteine residues. Very recently,  
36 the racemization step catalyzed by aspartate racemase has also been studied by means  
37  
38

of a QM/MM approach [24]. The calculated free energy barrier of 17.5 kcal/mol compares well with the experimental data and again the racemization process is described as concerted but highly asynchronous. However, the deprotonation process that forms the anionic cysteine is not even mentioned.

Glutamate racemases of several pathogenic bacteria, including *Helicobacter pylori* (HpMurI), have been recently characterized and their regulation mechanisms have been described [3]. HpMurI is an homodimer and shares a conserved topology and fold with the rest of MurI monomers. Each enzyme monomer is comprised of two domains that exhibit a pseudo-symmetry axis with catalysis taking place at the interface of those two domains. However, the active sites located at the interface of the two domains in each monomer are in a face-to-face orientation shielded from the solvent whereas BsRacE monomers oligomerize in a tail-to-tail orientation with active sites opposed and fully exposed to the solvent.

The aim of this paper is to carry out the first theoretical study of the catalytic mechanism of HpMurI in order to assert if the four-hydrogen transfer mechanism involving two neutral cysteines assisted by one deprotonated aspartate and one doubly protonated histidine residue is also plausible like in BsRacE. As indicated above, one of the most intriguing open key-questions in MurI/RacE activity is to understand how those enzymes manage to generate the so-called “reverse protonation state” (ionized cysteine) which is not the most thermodynamically favorable protonation state of those residues at the catalytic pH but which might represent an active form of the enzyme offering kinetic advantages.

## 2 Methods and Simulation Details

### 2.1 Initial Setup. Model and equilibration of the Michaelis complex

The initial structure was modeled from the 1.90 Å resolution X-ray crystal structure of the glutamate racemase enzyme from the bacteria *Helicobacter pylori* (Hp-MurI) with PDB code 2JFY [3]. This structure was crystallized with a racemic mixture of the substrate (DGL or GLU). Coordinates in the crystallographic file correspond to a dimer (which is the biologically active form of this enzyme), with 255 aminoacids per monomer and a DGL substrate molecule in each of the two active centers. In monomer 1 (MON 1) there are 136 crystallographic water molecules (XWAT), whereas in monomer 2 (MON 2) there are 211. The coordinates of the hydrogen atoms of the protein and the substrate were determined using the HBUILD facility in the program CHARMM [25, 26]. The protonation states of the titrable residues at pH=7 were assigned by the PROPKA 3.1 software package [27, 28] in the PDB2PQR website [29]. The predicted pK<sub>a</sub> value for His183 without substrate in the active site indicated that it should be represented as doubly protonated, which is coherent with its proposed catalytic role. In the case of the catalytic residues Cys70 and Cys181, the pK<sub>a</sub> values obtained for the two monomers of the crystal structure with the substrate bound are around 11 and 13, respectively, and without the substrate are around 9 and 12, respectively. Therefore, we protonated them. See further details in the Supporting Information (Figure S1).

The structure was solvated with an equilibrated orthorhombic box of TIP3P [30] water molecules, and it was neutralized with sodium counterions. The total number of atoms in the model is 59630 atoms.

Classical molecular dynamics simulations with periodic boundary conditions (PBC) in the isothermal-isobaric ensemble at 310 K and 1 atm were used to equilibrate the

system. The program CHARMM [25, 26] and the CHARMM27 force field [31] were used. A spherical cutoff of 13 Å together with a switching function to fade the interaction energy to zero were applied for the non-bonded interactions. To compute the contributions of long range electrostatic interactions the Particle Mesh Ewald method was used [32]. All bond lengths were constrained by SHAKE [33] and the dielectric constant was set to 1. The total length of the MD simulation carried out on this model of the HpMurI/DGL complex is 16 ns. Further details can be found in a reference to be published [34].

The chemical steps that constitute the global enzymatic reaction have been studied on the basis of 7 different starting structures. In addition to the crystallographic structure, 6 more structures generated at 500 ps, 1000 ps, 1500 ps, 2000 ps, 5000 ps, and 10000 ps, were selected along the MD simulation. MON 2 was chosen to study the reactivity because the previous MD results suggested that its configuration is suitable for catalysis [34]. All the selected structures accomplished the optimum values of the distances Asp7-O $\delta$ 1 - Cys70-S $\gamma$  and Cys70-H $\gamma$  - C $\alpha$ -DGL to be considered as reactive structures.

Next, a QM/MM model was built from each of the 7 structures. All the models contain 50 atoms in the QM region, including the side chains of Asp7, Cys70, Cys181, His183, and the DGL molecule in the active center of MON2. The QM/MM frontier was treated with the generalized hybrid orbital (GHO) method [35]. The GHO atoms were the  $\alpha$ -carbons of all quantum enzyme residues.

The QM/MM PES was calculated by using the AM1 Hamiltonian for the QM region for the first and last proton transfers, whereas the AM1-SRP (Specific Reaction Parameters) Hamiltonian developed by Major *et al.* [16] for the alanine racemase enzyme has been used to describe the two proton transfers involved in the DGL enantiomeric inversion. Test calculations (see Table S1 in reference [15]) on values of proton affinities for several model compounds showed that AM1 can be considered as

a valid quantum method for describing the first and last proton transfers. In addition that AM1-SRP Hamiltonian (see Supporting Information of reference 16) has been fitted to provide a quantitative approach for describing the enantiomeric inversion. The CHARMM27 force field was used for the MM region [31]. Water molecules were modeled with the TIP3P potential [30]. The QM/MM van der Waals interactions were recalibrated in reference [8] for this reaction and the optimized parameters were used in the present work.

## 2.2 Reaction Coordinates and Optimization Details

Reduced potential energy profiles of the different proton transfers that compose the global enzymatic reaction have been generated. Figure 1 shows schematically the atoms of the catalytic residues involved in each proton transfer.

The first reaction studied corresponds to the proton transfer from Cys70 to Asp7. The reaction coordinate used to define this 1D-profile is the antisymmetric combination of distances involving the sulfur of the Cys70 residue (Cys70-S $\gamma$ ), the proton bonded to it (Cys70-H $\gamma$ ) and one of the oxygens of the Asp7 carboxylate (Asp7-O $\delta$ 1). This reaction coordinate is labelled RC<sub>CD</sub>. The CD subscript indicates that the proton is driven from the cysteine (C) to the aspartate (D),

$$RC_{CD} = r_{C70S\gamma-C70H\gamma} - r_{C70H\gamma-D7O\delta 1} \quad (1)$$

Once the Cys70 sulfur is deprotonated the enantiomeric inversion of the glutamate is ready to be explored. In order to study it, two reaction coordinates are defined. RC1 describes the deprotonation of the H $\alpha$  of the substrate and involves the sulfur of Cys70, the  $\alpha$ -proton, and the  $\alpha$ -carbon atoms of the substrate,

$$RC1 = r_{H\alpha-C\alpha} - r_{C70S\gamma-H\alpha} \quad (2)$$

The RC2 reaction coordinate is defined as the antisymmetric combination of distances involved in the protonation of the  $\alpha$ -carbon by the  $\gamma$ -proton of Cys181,

$$RC2 = r_{C181S\gamma-C181H\gamma} - r_{C181H\gamma-C\alpha} \quad (3)$$

For the enantiomeric process a 1D-PES can be explored with the reaction coordinate RC4, defined as follows:

$$RC4 = RC1 + RC2 \quad (4)$$

Finally, the reprotonation of the Cys181 by His183 is studied with a 1D-profile with another antisymmetric combination of distances involving the  $\delta$ -proton and the  $\delta$ -nitrogen of His183 and the Cys181 sulfur,

$$RC_{HC} = r_{N\delta-H\delta} - r_{H\delta-C181S\gamma} \quad (5)$$

1D scans have been obtained by a series of geometry optimizations of the mobile part of the system in the presence of harmonic restraints applied on the different reaction coordinates previously defined. The RESD module in CHARMM was used to define the harmonic restraint terms of the form,

$$V_{RESD} = \frac{1}{2} K_{RESD} (RC - RC_{REF})^2 \quad (6)$$

where  $K_{RESD}$  is the restraining force constant, which was set equal to 2500.0 kcal/(mol $\text{\AA}^2$ ). The quantity  $RC_{REF}$  is the reference value of the reaction coordinate at each energy minimization calculation. Each minimization was carried out with a gradient tolerance of 0.001 kcal/(mol  $\text{\AA}$ ) with the ABNR algorithm. In these minimizations the reaction coordinate was projected out of the gradient. In all optimizations only the atoms of the residues that had at least one atom within an sphere

of 20 Å from the  $\alpha$ -carbon of the substrate in the starting structure were allowed to move. Thus, the system included 5321 mobile atoms and 53253 fixed atoms.

The conjugate peak refinement (CPR) algorithm [36] was used to find a smooth reaction path for the enantiomeric process (the two central proton transfers). Optimized structures from the 1D-PES were used as input for the CPR algorithm. The mobile part of the system and the electrostatic cutoff were the same as in the RESD minimizations. The CPR path has been displayed along the coordinate RC4.

### 3 Results and Discussion

#### 3.1 First Proton Transfer: From Cys70 to Asp7

The different potential energy profiles obtained with the seven QM/MM models for the proton transfer from the  $S\gamma$  atom of Cys70 to the  $O\delta 1$  atom of the carboxylate of Asp7 as a function of the reaction coordinate  $RC_{CD}$  are displayed in Figure 4 on the QM(AM1)/MM PES. In order to reduce hysteresis effects, the coordinate  $RC_{CD}$  was explored forward and backward several times. In all cases the potential energy profile converged in 2-4 cycles. In each case the line shown in Figure 4 and the structural analysis of the interactions along the proton transfer have been done with the final exploration. The negative values of the reaction coordinate correspond to the reactant region, when the shifting proton ( $H\gamma$ ) is still closer to the donor sulfur atom than to the acceptor oxygen atom, thus involving a neutral Cys70 residue and a negative Asp7.

The potential energy profile corresponding to the black line (crystal) in Figure 4 and the evolution of the atomic distances involved in the  $RC_{CD}$  coordinate are shown in Figure 4 (in blue the Asp7- $O\delta 1$  - Cys70- $H\gamma$  distance and in red the Cys70- $S\gamma$  - Cys70- $H\gamma$  distance). In addition, Table 1 shows the interaction distances between the substrate and the aminoacids in the active site along the proton transfer for the model

1  
2  
3  
4  
5  
6  
7  
8 crystal. Focusing on the behavior of the atoms involved in the reaction, the results  
9 indicate that before the proton transfer Ser8-HN interacts with Asp7-O $\delta$ 2 through a  
10 hydrogen bond (2.09 Å) that seems to be weakened at the end of the process (2.53  
11 Å). On the other hand, the decrease of the interaction distance between Ser8-HN and  
12 Cys70-S $\gamma$  suggests that, at the end of the process, Ser8 has replaced the interaction  
13 with Asp7 by the interaction with the now anionic Cys70 residue. In regards to the  
14 substrate, the interaction distances analysis indicates that the main chain carboxylate  
15 oxygens of DGL interact with the residues Asn71 and Thr72. The proton donor and  
16 proton acceptor atoms also interact with DGL through its -NH $_3^+$  group. However, the  
17 analysis of the interaction distances in Table 1 between Asp7-O $\delta$ 1 and Cys70-S $\gamma$  with  
18 DGL-NH $_3^+$  indicates that the movement of the ammonium group is not as sudden and  
19 significant as in the case of the BsRacE enzyme [15]. As already seen in the case of  
20 BsRacE the residue Asp7 is also interacting with a water molecule (XWAT:38).

21  
22  
23  
24  
25  
26  
27  
28  
29  
30 The potential energy barrier has a value of 11.6 kcal/mol and the reaction is  
31 exoergic by 1.9 kcal/mol, which in both cases are lower values than the ones obtained  
32 by us [15] for the BsRacE enzyme . It is reasonable to think that these differences  
33 in the reaction energy and barrier height are related to the different mechanism of  
34 negative charge stabilization that we have found when simulating the first proton  
35 transfer with the models based on the crystal structures of BsRacE and HpMurI.  
36 While in BsRacE the stabilization role is carried out by the DGL-NH $_3^+$  group, in  
37 HpMurI is the amide group of Ser8 which first forms a hydrogen bond with Asp7-O $\delta$ 1  
38 and, once this residue has abstracted the proton of Cys70, then it interacts with the  
39 Cys70-S $\gamma$  atom. The neutral amide group of Ser8 interacts with weaker interactions  
40 than the protonated DGL-NH $_3^+$  group of the substrate, whose stabilization effect was  
41 estimated [15] to be 10 kcal/mol. Ser8 is not able to form salt-bridge interactions, and  
42 thus, less energy is needed to break the interaction with Asp7-O $\delta$ 1 and less energy is  
43 released when after the proton transfer Ser8 forms a new interaction with Cys70-S $\gamma$ .  
44  
45  
46  
47  
48  
49  
50  
51  
52  
53  
54  
55  
56  
57  
58  
59  
60

The results obtained with the other models can be compared with the above commented results for the model crystal. As shown in Figure 4 the different starting structures result in different potential energy barriers, which can be classified in two groups. Structures generated at short simulation times (< 2 ns) and structures generated at long simulation times (> 2 ns). The former group (crystal, 500, 1000 and 1500) show barrier height values between 10.5 and 11.9 kcal/mol, whereas for the later group the values obtained are less homogeneous. Similar results, 13.4 kcal/mol and 14.6 kcal/mol are obtained for models 2000 and 5000, respectively, but a much lower value of the barrier height, 8.2 kcal/mol, is found for the model 10000. In addition, the reaction results to be isoergic, endoergic, and exoergic, depending on the model.

The analysis of the first proton transfer process in the seven models (see Tables S1 to S6 corresponding for the models 500, 1000, 1500, 2000, 5000, and 10000, in the Supporting Information) indicates that the substrate interacts with different conserved aminoacids in the active site, that is, Ser8, Tyr39, Gly40, Asn71, Thr72, and Thr182, through both the side chain and the main chain carboxylates. However, only in one of the models (crystal) the main chain -NH<sub>3</sub><sup>+</sup> group has a salt-bridge interaction with the catalytic residue Asp7 as the one found for the BsRacE enzyme. In the other models the stabilization role attributed to the -NH<sub>3</sub><sup>+</sup> group of the substrate in BsRacE is substituted by the enzymatic residue Ser8

Finally, in all cases we have found solvent molecules that interact with the atoms or residues involved in the reaction. Although these molecules present a high degree of variability and a dynamical behavior, the interactions found suggest a possible catalytic role of the solvent.

### 3.2 Enantiomeric inversion

Once the Cys70 residue is deprotonated, it is ready to abstract the H $\alpha$  atom from the DGL. The high number of hydrogen bonds that the aminoacids and water molecules form around the substrate facilitate the proton abstraction. Now, the question is whether the carbanionic intermediate generated is concertedly reprotonated by Cys181 or in a subsequent step.

The enantiomerization of DGL to GLU has been simulated for all the seven models by a series of restrained energy minimizations on the hybrid QM(AM1-SRP/MM) PES and using the RC4 reaction coordinate (Eq. 4). For each model, the starting structure was the product structure obtained when simulating the proton transfer between Cys70 and Asp7. Subsequently, the obtained reaction path has been refined with the CPR algorithm, using as initial search points the initial, final and some intermediate structures of the 1D-PES obtained with the geometric coordinate RC4.

However, only for three models (crystal, 500 and 5000) the minimum energy path and the transition state structures localized by the CPR algorithm were acceptable. The enantiomeric process simulated on the other four models resulted in a very high potential energy barrier with the exception of model 2000 which does not lead to products (see Fig. S2 in the Supporting Information), which is an indication that the starting structure was not reactive.

Figure 4 shows the minimum energy path obtained with the CPR algorithm for the models crystal, 500, and 5000 in a 2D-plot as a function of the deprotonation RC1 and reprotonation RC2 coordinates. The 2D-plot representation of the minimum energy reaction path in Figure 4 allows us to analyze the evolution of the interatomic distances along the process. Here, it is worthy to note that the use of the CPR algorithm has improved a lot the results obtained with the geometric reaction coordinate, as can be seen in Figure S3. The use of a more global reaction coordinate has reduced the hysteresis effect and, as a consequence, has reduced the barrier height

corresponding to the three system models by around 20 kcal/mol (Fig. 4).

Returning to Figure 4, it indicates that the CPR algorithm localizes two transition states for model 500, whereas only one transition state is found for the models crystal and 5000. However, the potential energy barrier height is very similar for the four transition states: 22 kcal/mol for the abstraction of the H $\alpha$  and 24 kcal/mol for the reprotonation of the C $\alpha$  in model 500, versus 25.3 and 25 kcal/mol for the only transition states found for models crystal and 5000, respectively. As for the potential energy of reaction, the three calculated paths give very similar values, that is, 1.0, 2.0, and -1.0 kcal/mol for models crystal, 500, and 5000, respectively.

## Energy profiles analysis: evolution of the reaction coordinate

The projection of the minimum energy path found on the two coordinates plane in Figure 4 allows us to analyze the evolution of the reactive bonds along the reaction. The reaction path followed for the system in model 500 is a step-wise process (see black line in Figure 4) where the proton abstraction from Cys70 to Asp7 occurs first, which causes the increase of the RC<sub>1</sub> coordinate from -1.5 to 1.5 Å, and arrives to a carbanionic intermediate structure (at approximately RC<sub>1</sub>=1.5 Å, RC<sub>2</sub>=-2.5 Å) that subsequently receives a proton from Cys181 and, as a consequence, the distance RC<sub>2</sub> increases from -2.5 to 1 Å. In contrast, we observe that the model crystal is a representation of the other mechanistic extreme because the optimized minimum energy path almost follows the diagonal line from reactant to products without passing through any intermediate. In between, we find model 5000, which, in spite of having a unique transition state, evolves asynchronously by advancing first the RC<sub>1</sub> coordinate and, after the transition state, the RC<sub>2</sub> coordinate. At this point, it is worthy to note that model 5000 behavior is in between the two lower time models what indicates that different degrees of synchronicity might be found at any time of the system evolution.

## Structural analysis of the 4 transition state structures

The four transition state structures found for the three models are shown in Figure 4, where we can see the values of the bond distances implied in the reaction at the TSs.

As already mentioned, the minimum potential energy paths found for the racemization process modeled with the models crystal and 5000 correspond to one-step mechanisms that go through a unique transition state structure located at around  $RC4 = 0 \text{ \AA}$  in each model (Fig. 4). These two transition state structures are shown in the upper part of Figure 4, where it can be seen that the distances from the  $\alpha$ -carbon of the carbanionic TS to the catalytic Cys70 and Cys181 respectively, are the same at each side of the  $\alpha$ -carbon, which reflects the symmetrical disposition of the two cysteines. The distances of Cys70-S $\gamma$  with respect to the leaving (deprotonation) proton and of Cys181-S $\gamma$  with respect to the incoming (reprotonation) proton are  $1.4 \text{ \AA}$  for both transition state structures. These values clearly indicate that at the region of the transition state the deprotonation process has nearly finished when the reprotonation process has just been initiated. In agreement, the distances between the  $\alpha$ -carbon and the leaving and incoming protons are longer than  $2.0 \text{ \AA}$ . The crystal model presents the shortest  $C_\alpha$ -H distances at the TS ( $2.0 \text{ \AA}$  compared to  $2.8 \text{ \AA}$  in the model 5000 TS), what results in a more compressed TS structure. On the other hand, the lower part of Figure 4 shows the two TS structures for the two reaction steps found in the racemization process modeled with the model 500. The first transition state structure (located at  $RC4 = -2.6 \text{ \AA}$ ) corresponds to the abstraction of the  $\alpha$ -proton by Cys70, and the second one (located at  $RC4 = 1.1 \text{ \AA}$ ) to the reprotonation of the  $\alpha$ -carbon by Cys181 at the other face of the carbanionic intermediate formed after the proton abstraction. Both TS structures found for the model 500 are asymmetric in regards to the  $C_\alpha$ -H distances, which is the expected trend for a two-step mechanism.

Another structural important aspect to analyze is the cyclic or extended nature of the TS structures found in this work, which is a question raised by Spies *et al.* in a recent paper about BsRacE [17]. In the mentioned paper, these authors ran MD simulations of two different models: the RacE/DGL complex, from the crystal structure, and the complex between RacE and the glutamate carbanion. All the snapshots obtained from the simulation with the DGL substrate were interpreted as not reactive, because of the proximity between the ammonium group of DGL and the thiolate sulfur atom of Cys74. It should be noted that the formation of this ionized cysteine was not discussed in this work. In contrast, the glutamate carbanion MD simulation gave snapshots that were classified as reactive and from them several TS structures where first found at the PM3 level and using small active-site models (clusters of less than 70 heavy atoms), and subsequently, two of them where further examined in QM/MM HF/6-31G(d,p)/OPLS geometry optimizations. In this case the entire system was included in the calculations. Transition states for proton transfer were located for both directions of the racemization reaction. The transition states found are in the cyclic form of glutamate, and the authors conclude that this is the only reactive form of the substrate. The cyclic structure is characterized by values of -47.5° for the dihedral N/C<sub>α</sub>/C<sub>β</sub>/C<sub>γ</sub> (versus 72.1° in the noncyclic form) and 83.6° (versus 59.3°) for the C<sub>α</sub>/C<sub>β</sub>/C<sub>γ</sub>/C<sub>δ</sub> dihedral. In contrast to these results, we have found that only two of the located TS structures presented in this work have dihedrals values that allow us to identify them as cyclic, that is, the TS structures found from the models 5000 and crystal. The evolution of the mentioned dihedral angles along the reaction coordinate is shown in Figures S4, S5, and S6 for the models crystal, 500, and 5000, respectively. Figures S4 and S6, indicate that the corresponding TS structures have values of -56.2° and 19.0°, respectively, for the N/C<sub>α</sub>/C<sub>β</sub>/C<sub>γ</sub> dihedral angle, and values of 105.0° and 81.4°, respectively, for the C<sub>α</sub>/C<sub>β</sub>/C<sub>γ</sub>/C<sub>δ</sub> dihedral angle, which in both cases correspond to values within

the limits that characterize the cyclic structure.

In contrast, Figure S5 shows dihedral angles values that highlight the extended nature of the structures generated for model 500 along the reaction path.

Finally, Figure 4 shows an overlapping of three of the four TS structures found. Concretely, the two transition states structures of the “two-base” mechanism found for model 500, in which the extended disposition of the backbone is clearly seen, contrast with the cyclic form of the model 5000 TS structure.

### 3.3 Last Proton Transfer: From His183 to C181

After the racemization of DGL → GLU, the catalytic Cys181 is deprotonated, which is not energetically favorable and, moreover, it is not the final state of the catalytic cycle. At the end of the enzymatic process, the system should be prepared to racemize the substrate in the opposite direction, from GLU to DGL. Thus, Cys181 has to take a proton from the solvent or, more probable, from an enzymatic residue. Previous experimental [6] and theoretical works [15] have demonstrated that His183 is a suitable candidate to give the proton to Cys181. Thus, for the three models, we have simulated the proton transfer from the  $\delta$  nitrogen of His183 to Cys181 by the use of the geometric reaction coordinate  $RC_{HC}$  defined in Equation 5. The final converged structure of the CPR profile corresponding to the previous step, the racemization reaction, was used to initiate this last proton transfer in the case of models crystal and 500. In both cases, the distance between the N $\delta$  atom of His183 and the S $\gamma$  atom of Cys181 was less than 3.0 Å at the end of the racemization, and the proton transfer reaction profile was initiated from values of  $RC_{HC}$  of -1.4 and -0.8 Å for the model 500 and crystal, respectively. However, in the case of the model 5000, the final structure at the end of the racemization has the side-chain of His183 looking at the opposite face of the active site. As a consequence, a series of energy minimizations were carried out with different values of the  $RC_{HC}$  reaction coordinate, from the final structure of

the CPR profile of the racemization in model 5000 to a minimized structure with a value of -1.8 Å. This last structure was taken as the reactant for the proton transfer from His183 to Cys181. It is worthy to note here that in the previous MD simulation at the reactant zone, the movement of the His183 side-chain between the two extreme configurations (facing or not the active site) was identified as a natural movement of this residue. This observation justifies that, in order to complete the study of the global reaction mechanism, we drive the system to a suitable reactant to start the simulation of the last proton transfer step. Figure 4 shows the three potential energy profiles for the three models. From this Figure it is clear that there is a correlation between the length and the height barrier of the path.

That is, the shortest path in the terms of  $\text{RC}_{\text{HC}}$  reaction coordinate (the one corresponding to the model crystal) results to have the smallest barrier (6 kcal/mol), whereas the path with larger distance between the reactants and products and the transition state (model 5000) presents the highest barrier (22.5 kcal/mol). Between these two cases which differ in 16.5 kcal/mol, we find model 500 with a barrier of 10.9 kcal/mol. However, in the case of the difference between reactants and products, no such a correlation is found. That is, models crystal and 5000 are almost isoergic (by 1 and 3 kcal/mol, respectively), whereas model 500 is endoergic by 7 kcal/mol. The analysis of the interactions along the proton transfer might help to understand these differences. Tables S10 and S11 show the variation of the interaction distances of the substrate with the active site residues and the solvent molecules for models 500 and 5000, respectively. In general, the interaction between enzymatic residues and the side and main chain atoms of the substrate do not change during the proton transfer reaction. In contrast, the solvent molecules play the role of stabilizing the negative charge on Cys181 at the beginning of the process and on His183 at the end of it. This is specially important in the case of model 5000, where, as suggested by the variation of the interaction distances of His183, the stabilization provided by WAT:8484 on the

product side makes the process plausible in spite of the high barrier. Interestingly, the fact that the orientation of His183 was opposite to the active site, seems to allow the presence of more water molecules in it, which in turn, provides a major stabilization to the catalytic and polar active site residues. Thus, the solvent molecules might assist the process in such cases.

## 4 Conclusions

In this paper we have carried out QM/MM calculations on the enzymatic mechanism of HpMurI that catalyzes the enantiomeric interconversion between DGL and GLU. The racemase reaction requires the abstraction of the GLU's  $\alpha$ -proton which has a high  $pK_a$ . Two optimally located cysteines play the role of acid/base catalytic residues in the two proton transfers required to invert the glutamate stereochemistry. The roles of those two cysteines have been demonstrated by experimental kinetic isotope effects and theoretical studies of that racemization in different racemases. However, there are several aspects of that mechanism that still need of further consideration and analysis. We have already reported that the  $pK_a$ s of the cysteine residues indicate that their stable protonation state in the enzyme active site corresponds to the neutral thiol. The question is then how the enzyme manages to deprotonate the catalytically active cysteines. Another aspect concerns the differences in quaternary structures that produce differences in the active sites of racemases among the various species. The question here is to which extent the catalytic mechanism depends on the enzyme species. Our results with HpMurI demonstrate that the four-transfer process found in BsRacE for converting DGL into GLU is also plausible in HpMurI. First, Asp7 deprotonates Cys70. Once Cys70 is deprotonated, the enantiomeric inversion of the  $\alpha$ -carbon involving two proton transfers (from the  $\alpha$ -carbon to Cys70 and from Cys181 to the  $\alpha$ -carbon) takes place. Finally, the nascent deprotonated Cys181 is

protonated by His183.

All the selected models taken from an MD simulation of the Michaelis complex DGL/HpMurI provide similar reaction paths for the first proton transfer between Cys70 and Asp7. Those results confirm that Asp7, which belongs to the group of strictly conserved residues, has the catalytic role of assisting the deprotonation of DGL by participating in general base catalysis with neutral Cys70 thiol. We also observed that catalytic role for the corresponding aspartic residue in both, ApMurI and BsRacE.

As for the enantiomeric inversion step, only three out of the seven models provided minimum energy paths and transition states with acceptable energetics (potential energy barriers in between 22 and 25 kcal/mol) compatible with the experimental value of  $k_{cat}$  [3] (see as a summary of the calculations corresponding to a different models the scheme in Figure S7). The structural analysis of the transition states corresponding to the racemization process showed a rather high variability. The enantiomeric inversion is either a one-step or a two-step process. In other glutamate racemases of different species (ApMurI, BsRacE) and in other racemases, the inversion is concerted but showing different degrees of asynchronicity. Another structural feature of the enantiomeric transition states of ApMurI is the cyclic or extended nature of the TS structures. In contrast, in the cyclic transition states the  $\text{NH}_3^+$  group forms intramolecular hydrogen bonds with the substrate's side-chain carboxylate. For BsRacE only the extended conformation was located in our previous work [15] whereas in Spies study *et al.* only the cyclic transition state was reported [17]. In this sense, this work demonstrates that somewhat different transitions state structures corresponding to the racemization step can be stabilized in the glutamate racemase active site.

To complete the catalytic cycle the Cys181 residue must be reprotonated. Our calculations show the viability that this last proton transfer takes place between His183 and Cys181, in agreement with experimental proposals and our results in

BsRacE, even though His183 side chain also visits configurations quite further away Cys181 along the MD trajectory.

The multiple QM/MM reaction path approach used in this work has been useful to account for protein dynamics and to investigate the effect of different conformations on the enzyme reaction energy barriers of the HpMurI catalytic mechanism. This approach has consisted of two main components: generating enzyme-substrate conformations with classical molecular dynamics simulations and mapping out the minimum reaction energy path for each chosen conformational snapshot with combined QM/MM calculations. It is found that enzyme-substrate conformation fluctuations lead to significant differences in the reaction energy barriers, in fact, from seven snapshots of the MD trajectory only three of them become reactive. In addition, the comparison between the three reactive pathways reveals the plasticity of glutamate racemase and how different catalytic agents may intervene to stabilize the transition state in a different way along the reaction path. Our study highlights the importance of employing multiple starting structures [37, 38, 39] in the QM/MM study of enzyme reactions and indicate that structural fluctuations are an integral part of the enzyme reaction process.

## Acknowledgment

We are grateful for financial support from the Spanish "Ministerio de Economía y competitividad" through project CTQ2011-24292, the "Generalitat de Catalunya" (2009SGR409), and the computational resources of Barcelona Supercomputing Centre through project BCV-2009-1-0023 and BCV-2009-1-0029. EM wants to thank the financial support of CONACYT (México) through fellowship No. 302244.

## Supporting Information Available:

Calculated  $pK_a$  values for catalytic residues, potential energy profiles and CPRs for the racemization process using different models of HpMurI, cyclic/extended nature of the transition state structures corresponding to the enantiomeric inversion, flux diagram of the methodological approach used, and important interactions found in the active site between the substrate, enzymatic residues and water molecules along the different processes of the whole catalytic reaction. This material is available free of charge via the Internet at <http://pubs.acs.org>.

## References

- [1] Dios, de A.; Prieto, L.; Martín, J. A.; Rubio, A.; Ezquerra, J.; Tebbe, M.; Uralde, de B. L.; Martín, J.; Sánchez, A.; LeTourneau, D. L.; McGee, J. E.; Boylan, C.; Parr, T. R.; Smith, M. C. *J Med Chem* **2002**, *45*, 4559.
- [2] Fisher, S. L. *Microbial Biotechnology* **2008**, *1*, 345.
- [3] Lundqvist, T.; Fisher, S. L.; Kern, G.; Folmer, R. H. A.; Xue, Y.; Newton, D. T.; Keating, T. A.; Alm, R. A.; Jonge, de B. L. M. *Nature* **2007**, *447*, 817.
- [4] Tanner, M. E.; Gallo, K. A.; Knowles, J. R. *Biochemistry* **1993**, *32*, 3998.
- [5] Glavas, S.; Tanner, M. E. *Biochemistry* **1999**, *38*, 4106.
- [6] Glavas, S.; Tanner, M. E. *Biochemistry* **2001**, *40*, 6199.
- [7] Tanner, M. *Accounts of Chemical Research* **2002**, *35*, 237.
- [8] Puig, E.; Garcia-Viloca, M.; González-Lafont, A.; Lluch, J. M. *J Phys Chem A* **2006**, *110*, 717.
- [9] Puig, E.; Garcia-Viloca, M.; Gonzalez-Lafont, A.; Lopez, I.; Daura, X.; Lluch, J. *J. Chem. Theory Comput* **2005**, *1*, 737.
- [10] Puig, E.; Garcia-Viloca, M.; Gonzalez-Lafont, A.; Lluch, J. M.; Field, M. J. *J. Phys. Chem. B* **2007**, *111*, 2385.
- [11] Richard, J.; Williams, G.; O'Donoghue, A.; Amyes, T. *Journal of the American Chemical Society* **2002**, *124*, 2957.
- [12] Richard, J.; Amyes, T. *Bioorganic Chemistry* **2004**, *32*, 354.
- [13] Hwang, K.; Cho, C.; Kim, S.; Sung, H.; Yu, Y.; Cho, Y. *Nature Structural Biology* **1999**, *6*, 422.

- 1  
2  
3  
4  
5  
6  
7  
8 [14] Ruzheinikov, S.; Taal, M.; Sedelnikova, S.; Baker, P.; Rice, D. *Structure* **2005**,  
9 13, 1707.
- 10  
11  
12 [15] Puig, E.; Mixcoha, E.; Garcia-Viloca, M.; González-Lafont, A.; Lluch, J. M. *J Am Chem Soc* **2009**, 131, 3509.
- 13  
14  
15  
16 [16] Major, D. T.; Gao, J. *J. Am. Chem. Soc.* **2006**, 128, 16345.
- 17  
18  
19 [17] Spies, M. A.; Reese, J. G.; Dodd, D.; Pankow, K. L.; Blanke, S. R.; Baudry, J. *J Am Chem Soc* **2009**, 131, 5274.
- 20  
21  
22  
23 [18] Whalen, K. L.; Pankow, K. L.; Blanke, S. R.; Spies, M. A. *ACS medicinal chemistry letters* **2010**, 1, 9.
- 24  
25  
26  
27 [19] Whalen, K. L.; Tussey, K. B.; Blanke, S. R.; Spies, M. A. *Journal of Physical Chemistry B* **2011**, 115, 3416.
- 28  
29  
30 [20] Sims, P.; Larsen, T.; Poyner, R.; Cleland, W.; Reed, G. *Biochemistry* **2003**, 42, 8298.
- 31  
32  
33 [21] Spies, M.; Toney, M. *Biochemistry* **2003**, 42, 5099.
- 34  
35  
36 [22] Spies, M. A.; Toney, M. D. *Journal of the American Chemical Society* **2007**, 129, 10678.
- 37  
38  
39 [23] Rubinstein, A.; Major, D. T. *Journal of the American Chemical Society* **2009**, 131, 8513.
- 40  
41  
42 [24] Zhang, C.; Guo, Y.; Xue, Y. *Theoretical Chemistry Accounts* **2011**, 129, 781.
- 43  
44  
45 [25] Brooks, B. R.; Bruccoleri, R. E.; Olafson, B. D.; States, D. J.; Swaminathan, S.; Karplus, M. *Journal of Computational Chemistry* **1983**, 4, 187.

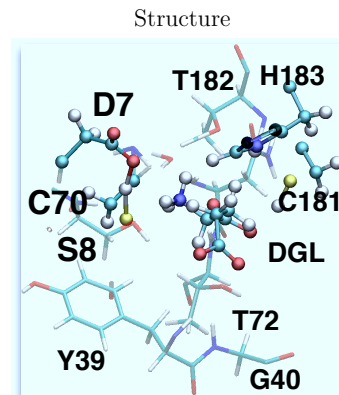
- [26] Brooks, B. R.; Brooks, C. L.; Mackerell, A. D.; Nilsson, L.; Petrella, R. J.; Roux, B.; Won, Y.; Archontis, G.; Bartels, C.; Boresch, S.; Caflisch, A.; Caves, L.; Cui, Q.; Dinner, A. R.; Feig, M.; Fischer, S.; Gao, J.; Hodoscek, M.; Im, W.; Kuczera, K.; Lazaridis, T.; Ma, J.; Ovchinnikov, V.; Paci, E.; Pastor, R. W.; Post, C. B.; Pu, J. Z.; Schaefer, M.; Tidor, B.; Venable, R. M.; Woodcock, H. L.; Wu, X.; Yang, W.; York, D. M.; Karplus, M. *Journal of Computational Chemistry* **2009**, *30*, 1545.
- [27] Li, H.; Robertson, A. D.; Jensen, J. H. *Proteins* **2005**, *61*, 704.
- [28] Olsson, M. H. M.; Søndergaard, C. R.; Rostkowski, M.; Jensen, J. H. *Journal of Chemical Theory and Computation* **2011**, *7*, 525.
- [29] Dolinsky, T. J.; Nielsen, J. E.; McCammon, J. A.; Baker, N. A. *Nucleic Acids Research* **2004**, *32*, W665.
- [30] Jorgensen, W.; Chandrasekhar, J.; Madura, J.; Impey, R.; Klein, M. *The Journal of Chemical Physics* **1983**, *79*, 926.
- [31] MacKerell, A. D.; Banavali, N.; Foloppe, N. *Biopolymers* **2000**, *56*, 257.
- [32] Essmann, U.; Perera, L.; Berkowitz, M.; Darden, T.; Lee, H.; Pedersen, L. *J Chem Phys* **1995**, *103*, 8577.
- [33] Ryckaert, J.-P.; Cicotti, G.; Berendsen, H. J. C. *Journal of Computational Physics* **1977**, *23*, 327 .
- [34] Mixcoha, E.; Garcia-Viloca, M.; González-Lafont, A.; Lluch, J. *To be published elsewhere* **2012**,
- [35] Gao, J.; Amara, P.; Alhambra, C.; Field, M. J. *The Journal of Physical Chemistry A* **1998**, *102*, 4714.

- 1  
2  
3  
4  
5  
6  
7  
8 [36] Fischer, S.; Karplus, M. *Chem. Phys. Lett.* **1992**, *194*, 252.  
9  
10 [37] Thorpe, I. F.; Brooks, C. L. *Journal of Physical Chemistry B* **2003**, *107*, 14042.  
11  
12 [38] Zhang, Y.; Kua, J.; McCammon, J. *Journal of Physical Chemistry B* **2003**, *107*,  
13  
14 4459.  
15  
16 [39] Hu, P.; Zhang, Y. *Journal of the American Chemical Society* **2006**, *128*, 1272.  
17  
18  
19  
20  
21  
22  
23  
24  
25  
26  
27  
28  
29  
30  
31  
32  
33  
34  
35  
36  
37  
38  
39  
40  
41  
42  
43  
44  
45  
46  
47  
48  
49  
50  
51  
52  
53  
54  
55  
56  
57  
58  
59  
60

## Tables

Table 1: Interaction distances between the aminoacids, the solvent, and the substrate along the first proton transfer for the model crystal

Interaction		Distance (Å)		
Atom <sub>1</sub>	Atom <sub>2</sub>	Initial	T.S.	Final
D7-O <sub>δ2</sub>	XWAT:38-H	1.82	1.94	1.85
D7-O <sub>δ2</sub>	S8-HN	2.09	2.58	2.53
D7-O <sub>δ1</sub>	DGL-NH <sub>3</sub> <sup>+</sup>	2.69	2.75	2.75
DGL-O <sub>τ1</sub>	N71-HN	1.98	1.96	1.90
DGL-O <sub>τ1</sub>	T72-HN	1.80	1.82	1.87
C70-S <sub>γ</sub>	S8-HN	3.32	2.48	2.80
C70-S <sub>γ</sub>	DGL-NH <sub>3</sub> <sup>+</sup>	3.62	3.23	3.03



## Figures Captions

**Figure 1:** Schematic representation of HpMurI active site. The colored arrows indicate the four steps of the catalytic mechanism. The first proton transfer from C70 to D7 in green, the proton abstraction and reprotonation of the  $\alpha$ -carbon in red, and the last proton transfer from H183 to C181 in blue. In all Figures and Tables the aminoacids are represented with the one-letter code.

**Figure 2:** Potential energy profiles of the proton transfer from Cys70 to Asp7 for all the studied models

**Figure 3:** Potential energy profiles of the proton transfer from Cys70 to Asp7 for the model crystal together with the evolution of the catalytic distances

**Figure 4:** CPR profile for the models crystal, 500, and 5000

**Figure 5:** Transition state structures found with the three models of the enzymatic system

**Figure 6:** Overlapping of the transition state structures found for models 500 and 5000

**Figure 7:** Potential energy profiles of the proton transfer from His183 to Cys181 for the different models

## Figures

Figure 1:

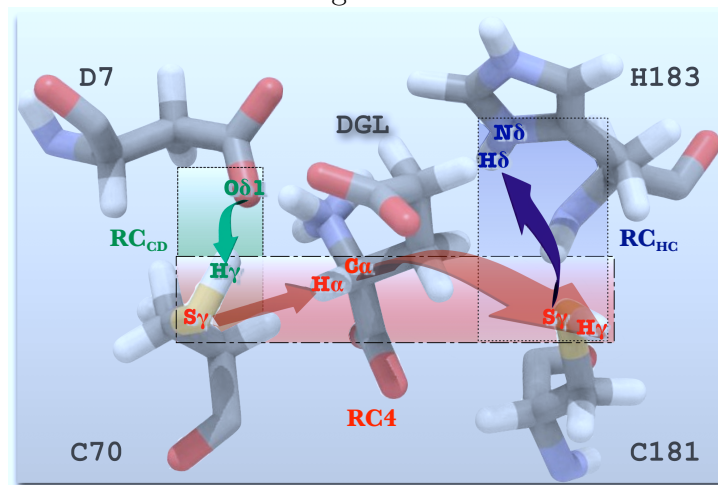


Figure 2:

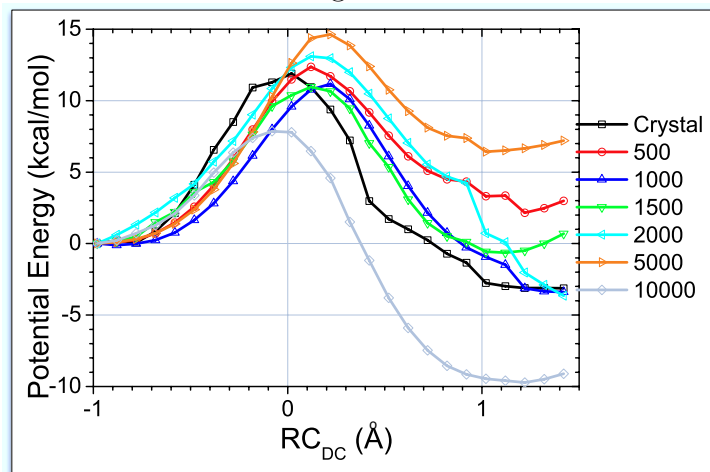


Figure 3:

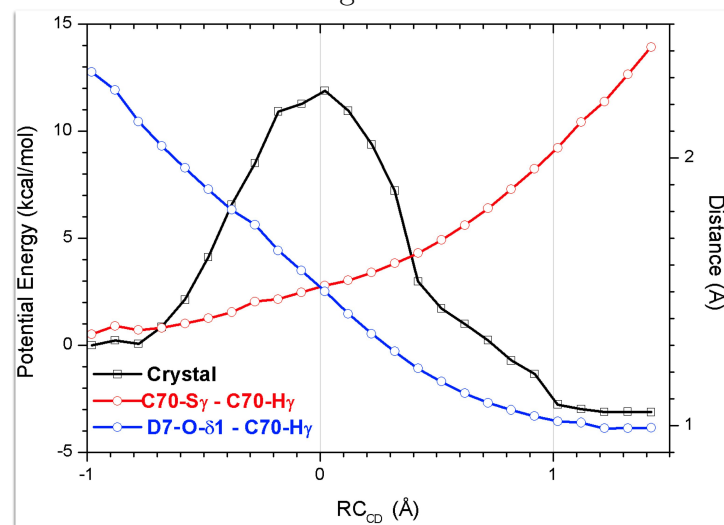


Figure 4:

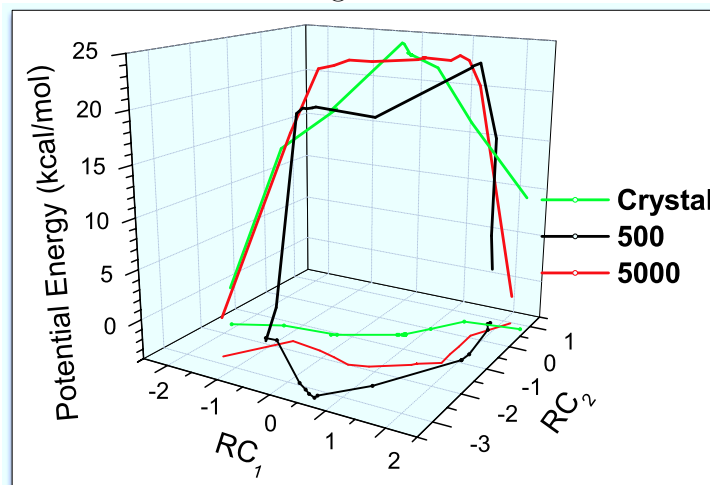


Figure 5:

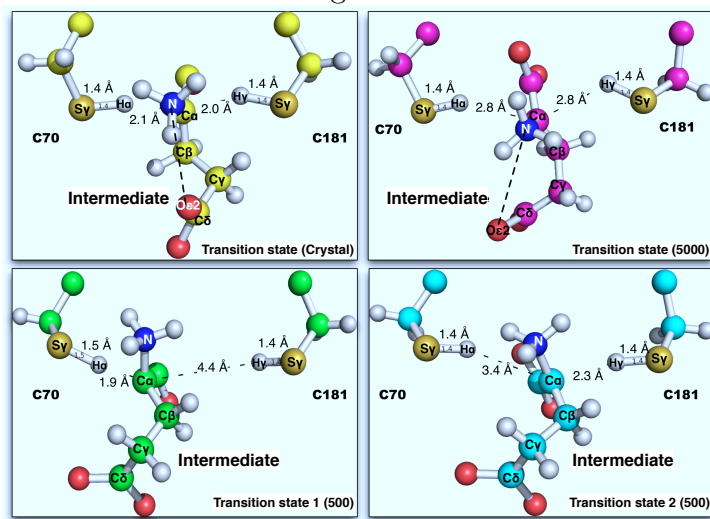


Figure 6:

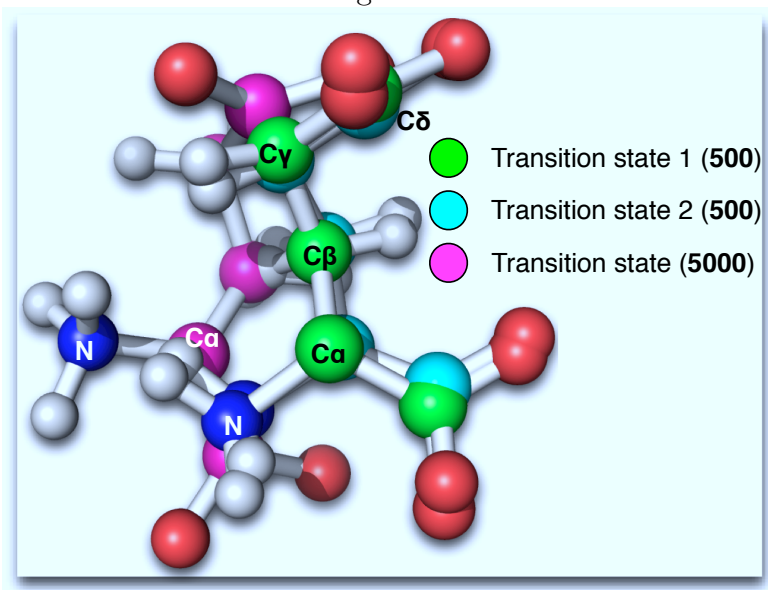
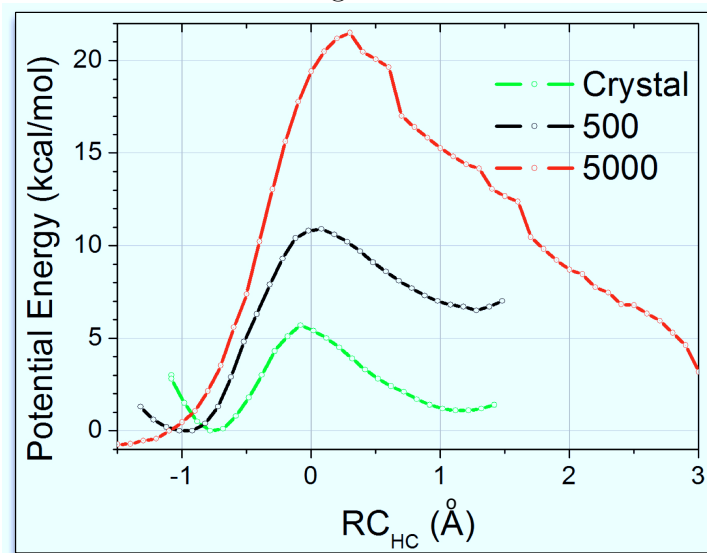


Figure 7:



## TOC

